

25

**NASA TECHNICAL
MEMORANDUM**

NASA TM X-52275

NASA TM X-52275

FACILITY FORM 602	67-21393 <small>(ACCESSION NUMBER)</small>	_____ <small>(THRU)</small>
	10/18/67 <small>(PAGES)</small>	_____ <small>(CODE)</small>
	TM-X-52275 <small>(NASA CR OR TMX OR AD NUMBER)</small>	28 <small>(CATEGORY)</small>

**STATUS OF THE 260-INCH DIAMETER SOLID
ROCKET MOTOR PROGRAM**

by Carl C. Ciepluch
Lewis Research Center
Cleveland, Ohio

TECHNICAL PAPER proposed for presentation at Second Solid
Propulsion Conference sponsored by the Interagency Chemical
Rocket Propulsion Group and the American Institute of
Aeronautics and Astronautics
Anaheim, California, June 6-8, 1967

STATUS OF THE 260-INCH DIAMETER SOLID ROCKET MOTOR PROGRAM

by Carl C. Ciepluch

Lewis Research Center
Cleveland, Ohio

TECHNICAL PAPER proposed for presentation at

Second Solid Propulsion Conference
sponsored by the Interagency Chemical Rocket Propulsion Group
and the American Institute of Aeronautics and Astronautics
Anaheim, California, June 6-8, 1967

NATIONAL AERONAUTICS AND SPACE ADMINISTRATION

STATUS OF THE 260 INCH-DIAMETER SOLID ROCKET MOTOR PROGRAM

by Carl C. Ciepluch

Lewis Research Center
National Aeronautics and Space Administration
Cleveland, Ohio

SUMMARY

The progress made toward the third 260-inch diameter solid propellant rocket motor (260 SL-3) test firing is reported. The 260 SL-1 case has been refurbished, rehydrottested and reinsulated. Development of a 50% higher burn rate propellant than that used in 260 SL-1 and SL-2 has been completed. The propellant incorporates a new and more effective burn rate catalyst. Processability of the propellant remains very similar to the previous propellant. Some degradation in propellant mechanical properties has been encountered. Fabrication of nozzle ablatives is nearing completion and fabrication of the nozzle shell and entrance ring has been completed. A cold flow aerodynamic investigation of the 260 SL-3 nozzle geometry has revealed the presence of high velocity circumferential flows behind the submerged nozzle entrance section. This is attributed to the asymmetric nozzle entrance flow emanating from the star port geometry. Motor tail-off is to be controlled by the use of inert slivers. A study of the optimum inert sliver size has indicated that the sliver should replace about 1% of the motor propellant.

INTRODUCTION

The 260-inch diameter solid propellant motor program was initiated by the Air Force in June of 1963. The objective of this initial effort was to demonstrate the feasibility of the 260-inch diameter motor. Major milestones were accomplished during this feasibility program by the successful test firing of two identical short-length 260-inch motors (260 SL-1 and SL-2) by the Aerojet-General Corporation in September of 1965 and February of 1966. These motors developed a maximum thrust of 3,500,000 pounds, with a web action time of about 114 seconds.

Development of 260-inch motor technology is continuing and a third motor test firing is planned. This motor, designated 260 SL-3, will produce a maximum thrust of about 5,400,000 pounds with a web action time of 75.2 seconds. The major technical areas being investigated in this program are: the design, fabrication, and performance of very large submerged ablative nozzles; high burn rate propellant suitable for large solid rocket motor processing; and thrust tail-off control. The motor program was initiated in March of 1966 and the motor test firing is scheduled for June of 1967. The Aerojet General Corporation is the prime contractor for the motor.

The object of this paper is to present the design philosophy and development and fabrication progress to date.

RESULTS AND DISCUSSION

The design, fabrication and test firing of the third 260-inch diameter, short length, solid propellant rocket motor (260 SL-3) is aimed at advancing the technology of large solid rocket motors in three main areas. One of the technical areas being investigated is the design, fabrication and performance of very large, submerged, ablative nozzles. The nozzle throat diameter is 89 inches which approaches the size appropriate for a full length 260-inch motor nozzle. The submerged nozzle concept offers advantages due to a reduction of nozzle length and reductions in ablative requirements and consequently cost. This type nozzle permits a wider selection of potential thrust vector control systems for the 260-inch motor. Thus, the fabrication problems and performance associated with a submerged nozzle design on a scale equivalent to that of the full length 260-inch motor are being investigated in this program.

A second technology area being investigated concerns high burn rate propellants. Advanced grain designs for 260-inch diameter solid rocket boosters will require propellant burn rates significantly higher than that developed for the 260 SL-1 and SL-2 motors. It is desirable that the required increase in propellant burn rate be obtained without unacceptable compromise in the processability, mechanical properties and cost of the propellant. The trade-off of these factors has guided the propellant development for the 260 SL-3 motor.

Finally, thrust tail-off control has been incorporated into the motor. The method of thrust tail-off control used in this program was the incorporation of inert propellant slivers. This method was chosen because of the current grain design, the relative simplicity of the system and the previously demonstrated effectiveness of this technique in smaller motors.

The ballistic performance characteristics and some design details of the 260 SL-3 motor are listed in table I. The maximum thrust of the motor is estimated to be 5.37×10^6 pounds. Because of the reuse of the 260 SL-1 case and core, the increased burn rate results in a reduction in motor web action time from 115 seconds for 260 SL-1 and SL-2 to a predicted 75.2 seconds for the SL-3 motor. The 260 SL-3 motor is shown in figure 1. The following sections describe in detail the main components of the motor.

Case

The 260 SL-1 case is being reused for the SL-3 motor test. The case was previously hydrotested at 737 psig in March of 1965 and test fired in September of 1965. All the barrel section insulation had to be removed and the metal surfaces were then sandblasted to remove the remaining insulation adhesive. A reinspection of the longitudinal welds by radiograph, ultrasonics and magnetic particles was made and revealed no significant changes in known defects nor generation of new defects. On September 28, 1966 the chamber was successfully rehydrotested, at the Aerojet Dode plant, to a maximum pressure of 707 psig or about 20% above maximum nominal operating pressure.

No anomalous behavior was noted during the test. Analysis of the strain gage data indicated that the response to the stress was as expected. The results of the hydrotest are reported in reference 1.

Insulation

The case barrel section insulation was damaged beyond repair during heat soak after the 260 SL-1 test firing. It was therefore removed and replaced with the same type insulation (V-44) using the same techniques that were used previously. Visual inspection of the insulation remaining in the aft and head domes revealed that it was intact and sufficient thickness remained to withstand a second firing. Adequate insulation thickness and bonding of the dome segments was confirmed during removal and replacement of the dome segment seam insulation. Some insulation buildup at the aft flange was required in order to mate with the nozzle insulation and this was accomplished using the trowellable (V-61) seam insulation. A photograph of the insulation process is shown in figure 2.

Ignition

Ignition will be accomplished with the same size aft-end ignitor as used on the previous motors. However, because of the larger throat diameter, the ignitor gas based on theoretical calculations, will penetrate 61 percent into the chamber free volume compared to 70 percent in the earlier firings. This is not expected to have a significant effect on the 260 SL-3 ignition, because this degree of ignitor gas penetration has been found to be more than adequate for ignition in other experimental programs.

Propellant

The design propellant burn rate for the 260 SL-3 motor is 0.71 inch per second or about a 50% increase above that for the previous motors. In order to achieve this burn rate with the previous propellant, it would have required the use of a prohibitively large percentage of finely ground oxidizer. This is illustrated in figure 3 where propellant burn rate as a function of coarse to fine oxidizer blend is shown for a 1% iron oxide burn rate catalyst concentration. Iron oxide concentrations about 1% are ineffective in increasing propellant burn rate, and therefore, a coarse to fine oxidizer blend in the neighborhood of 20/80 is required to achieve the desired burn rate. This level of fine oxidizer would have degraded propellant processability to an unacceptable level and also significantly complicated oxidizer grinding and handling. A more effective burn rate catalyst was required in order to keep the fine oxidizer concentration to a minimum for good processing. The one that was selected consisted of a combination of equal quantities of iron blue and BRA101 (an Aerojet proprietary compound). It can be seen in figure 3 that at a 1% catalyst level the required uncured propellant burn rate of 0.67 is attained with an oxidizer blend ratio of about 70/30 which is the same as used in the SL-1 and SL-2 propellant.

Propellant processed with the new burn rate catalyst in laboratory batch sizes proved to exhibit such high viscosity that propellant casting appeared unfeasible. This was traced to an interaction between the burn

rate catalyst and the dodecenyyl succinic anhydride polymer component. Removal of the anhydride component, along with the incorporation of a cure catalyst (FEAA) to improve cure rate, resulted in a significant improvement in the propellant viscosity and satisfactory cure characteristics. Evaluation of the modified propellant produced with the production facilities resulted in the necessity to increase the iron blue-BRA101 burn rate additive to 1.3% and a change in oxidizer blend ratio to 65/35 (coarse/fine) in order to meet the burn rate requirement.

The rate of viscosity buildup for the SL-3 propellant is shown in figure 4. It can be seen that the SL-3 propellant viscosity is greater than that for the SL-1 and SL-2 motors, and the viscosity slightly exceeds the desired 15,000 poise limit at 10 hours. Low viscosity is an important propellant property for the nonvacuum type of propellant casting that is necessary for large monolithic solid rocket motors. Therefore, in order to evaluate further the castability of the propellant prior to the actual motor loading, a subscale motor (44-in. diameter) was cast. The casting operation proceeded without difficulty using similar large motor casting techniques and after propellant cure, a radiographic examination of the propellant revealed no anomalies in the propellant or the propellant to insulation bond. As a result of this data the propellant processability was considered satisfactory. The propellant tensile and strain mechanical properties are shown in table II. It is apparent that the increased propellant burn rate has resulted in a moderate reduction in mechanical properties from that of the previous propellant. These lower propellant mechanical properties are not expected to have a serious impact on propellant grain structural margins. Conversely, the long term strain capability of the propellant was found to be improved over that of the previous SL-1 and SL-2 propellant. This is illustrated in figure 5 where one week constant strain data is presented.

Nozzle

The 260 SL-3 ablative nozzle design is based on previous experience with the SL-1 and SL-2 ablative nozzles. A cross section of the nozzle geometry showing the ablative component arrangement is shown in figure 6. Ablative materials for specific areas are generally the same as used previously except for the exit cone where the silica-phenolic tape has replaced carbon-phenolic tape in the area ratio range from 2.5 to 3.0. The nozzle area ratio was limited to 3.78 for reasons of economy and the fact that erosion is much less severe at high nozzle expansion ratios. The required ablative thicknesses were determined using the data from the earlier SL-1 and SL-2 nozzle firings because this resulted in greater ablative thicknesses than a computer prediction. The total design thickness was found by summing erosion multiplied by a safety factor, char heat effected zone and overwrap thicknesses. To correct the local erosion rate for chamber pressure differences, the following relation was used

$$\text{SL-3 erosion rate} = \text{SL-1 erosion rate} \left(\frac{P_{\text{SL-3}}}{P_{\text{SL-1}}} \right)^{0.8}$$

The total erosion thickness loss was then found by multiplying the cor-

rected erosion rate by the web action time. Erosion safety factors of 3, 2, and 1.5 were applied in the nose, throat and exit cone areas, respectively. The ablative materials and laminate orientation are indicated in figure 6.

Experience with large submerged ablative nozzles in previous Air Force programs (ref. 2) has indicated that erosion rates in the nose area and backside of the submerged entrance section have in some cases greatly exceeded prediction. These results plus the fact that the SL-3 nozzle entrance flow will be highly asymmetric due to the star type grain port immediately ahead of the nozzle contributed to a significant degree of uncertainty about the ablative performance in the region of the submerged entrance. As a result, two supporting experiments were performed to investigate these conditions; the first was a cold-flow aerodynamic study and the second was a hot firing of a subscale nozzle.

The cold-flow aerodynamic flow study was conducted at the Lewis Research Center using 1/14.2 scaled model of the SL-3 nozzle and aft-end grain geometry. The results of this study are also being presented at this meeting and therefore only a brief summary of the study will be presented here along with a discussion of the impact on the SL-3 nozzle design. A schematic drawing of the cold flow test rig is shown in figure 7. A plexiglas aft section allowed photographic observation of tufts placed behind the submerged lip. A photograph showing the tuft position during actual operation is shown in figure 8. It can be seen, as illustrated by the arrows, that the flow emanating from the grain valleys enters the cavity behind the submerged lip, turns and flows circumferentially towards the area behind the grain star points. The flow then turns toward the grain star points moving in an upstream direction toward the submerged nozzle entrance whereupon it flows over the entrance nose and is discharged thru the nozzle. The Mach number profiles existing behind the submerged lip are illustrated in figure 9. It can be seen that the Mach number reached nearly 0.2 at the extreme end of the cavity behind the submerged nozzle entrance. Examination of the Mach numbers with a grain shape that simulated 1/3 of the web action time completed showed that a maximum Mach number of 0.1 still existed. It was, therefore, apparent that high velocities would exist for most of the motor duration. In order to alleviate the circumferential flow, tests were made with the blunt aft-end grain surfaces aerodynamically faired. This fairing did not relieve the problem sufficiently and consequently additional rubber insulation and carbon tape were added behind the submerged nozzle entrance, as indicated in figure 6, in order to improve ablative safety factors in marginal areas. The Mach number profiles on the inside of the submerged section revealed no significant anomalies except for a slight decrement in flow velocity behind the propellant star points.

The subscale nozzle test will be made using a 44-inch diameter Minute Man case loaded with propellant processed during the qualification of the SL-3 propellant ingredients. The nozzle throat diameter will be about 15 inches and the action time will be 17 seconds. The nozzle will be an exact geometric subscale of the SL-3 nozzle design and the materials and method of fabrication will also be the same as those used in fabrication of the full scale nozzle. The aft-end grain

shape will also be closely simulated. This test, that will be conducted in March of 1967, is designed to determine whether any anomalous erosion performance will be encountered due to either ablative design and fabrication techniques or propellant grain and nozzle aerodynamic effects. These results will be considered in a final evaluation of the SL-3 nozzle.

The nozzle ablative components at this writing are all either completed or in some stage of fabrication. No major difficulties have been encountered, however, the usual fabrication discrepancies common to large ablatives have been encountered. Experience to date has indicated that a more fundamental knowledge of ablative fabrication process controls and techniques is desirable in order to build these expensive components on a more reliable basis.

The nozzle steel shell and the support for the nozzle entrance section have been built. The 200 grade 18% nickel maraging steel shell was fabricated by adding a new aft section to the salvaged fore-end section (including flange) of the SL-1 nozzle shell. These two pieces were joined by a girth weld. Prior to the SL-3 nozzle shell welding, a weld development program (NAS-3-7965) was conducted in order to determine acceptable weld and weld repair techniques for aged 200 grade maraging steel plate. This study revealed that the same welding techniques and aging cycle could be used for aged plate as had been used for the unaged plate. The mechanical properties and toughness of the weld made in aged plate were as good as those made in unaged plate. No hydrotest of the nozzle shell is planned prior to the motor test firing. The nozzle exit cone structural member consisted of composite of glass cloth and glass filament roving.

Thrust Tail-Off Control

In order to determine the proper size of inert sliver for effective thrust tail-off control of 260-inch diameter motors, an analytical study was made at Lewis (ref. 3). This study was based primarily on sliver effect on performance, however, it is also recognized, but not investigated here, that other vehicle considerations may also influence sliver size. The basic vehicle in this study consisted of a 3/4 length 260 inch motor booster and a SIVB second stage. Details of this vehicle are described in reference 4. The 260-inch motor contained a total of 2.4×10^6 pounds of propellant, and thrust tail-off characteristics similar to the 260 SL-1 and SL-2 motors were used. The pressure-time variation during tail-off of the motor is shown in figure 10. Also, indicated in the figure is the total propellant consumed at various times into the tail-off. The motor thrust during tail-off varies directly with chamber pressure.

Vehicle payload was calculated for a range of propellant weights consumed. During the calculations when the given weight of propellant consumed was reached, the thrust was instantaneously decreased to zero and stage separation sequence commenced. The remaining unused propellant or sliver was carried as inert booster weight during the calculations. The effect of inert sliver density and propellant consumed on payload is shown in figure 11. Also shown in the figure is the payload

capability for the case of no thrust tail-off. In this calculation an ideal case was assumed where all the propellant was burned at the nominal chamber pressure followed by an instantaneous pressure and thrust decay to zero. The ideal case provides an 8% increase in payload over the optimum payload for a sliver density of 0.028 lb/in.³. As can be seen in figure 11, there is an optimum weight of propellant consumed for maximum payload for each sliver density. The reason for the maximum results from two competing factors. First, as more propellant is consumed, payload increases due to the larger stage total impulse. However, increasing the total propellant consumed during tail-off also results in substantially lower thrust output and the point is eventually reached where gravity losses overcome the increased stage total impulse and payload decreases. Lower sliver densities increase payload by virtue of the increase in stage propellant mass fraction. One noteworthy conclusion from this study is that instantaneous tail-off improves payload performance and also eliminates the need for slivers. Tail-off control by means of grain design is therefore a desirable goal provided other disadvantages are not encountered.

The inert sliver composition was selected for the SL-3 motor primarily on a basis of obtaining good processability and mechanical properties. The composition consisted of 80% by weight of PBAN type binder and 10% each of antimony trioxide and asbestos fillers. The density of this sliver composition was about 0.039 lb/in.³. From figure 11, it is seen that the optimum propellant consumed is 99% for this density. The sliver size is therefore that required to replace the last 1% of propellant. A cross-sectional view of the required sliver profile is shown in figure 14. Since the propellant cross section is practically constant throughout the length of the motor, the sliver profile was made constant. The slivers were cast in 10 foot long molds and subsequently bonded to the case insulation. The calculated effect of the slivers on pressure time variation during tail-off is shown in figure 15. The actual effect of the slivers will be evaluated during the static test firing of the SL-3 motor.

SUMMARY OF RESULTS

The following summarizes the program made to date on the design, development and fabrication of the 260 SL-3 solid propellant rocket motor.

1. The 260 SL-1 case has been refurbished, rehydrottested and re-insulated.

2. The development of a propellant with a 50% higher burn rate than that used in the 260 SL-1 and SL-2 motors is completed. The increased burn rate propellant has resulted in a degradation in propellant mechanical properties and an increase in the propellant viscosity. However, this is not expected to have a sensing implication in either the propellant structural integrity or ease of processing and casting the propellant.

3. Fabrication of nozzle ablatives is nearing completion. The nozzle shell and submerged entrance support member have been fabricated.

4. A cold-flow aerodynamic study of the 260 SL-3 nozzle geometry has indicated that circumferentially induced flow velocities approaching a Mach number of 0.2 exist behind the submerged entrance section. As a result the original nozzle design has been modified to increase the erosion safety margin in marginal areas.

5. Motor tail-off control will be obtained by the use of inert slivers. The slivers have been sized to replace about 1% of the motor propellant.

REFERENCES

1. Anon., "Hydrostatic Test of 260 SL-3 Motor Chamber and Nozzle Shell," Aerojet-General Corporation, Report HTR-1, Contract NAS3-7998 (November 11, 1966).
2. Stutzman, R. D., Rafael, F., and Andrepont, W. C., "Performance Summary of 156-inch Diameter Solid Rocket Motors," ICRPG/AIAA Solid Propulsion Conference, CPIA Publ.-111, vol. 1 (June 1966), p. 209.
3. Rambler, J. R. and Thompson, R. L., Private Communication.
4. Dawson, R. P., "Saturn 1B Improvement Study Solid First Stage. Vol. 2," Douglas Aircraft Co., SM-47043, vol. 2 (NASA CR-67716) (Feb. 24, 1965).

TABLE I. - 260 SL-3 DESIGN AND PERFORMANCE CHARACTERISTICS

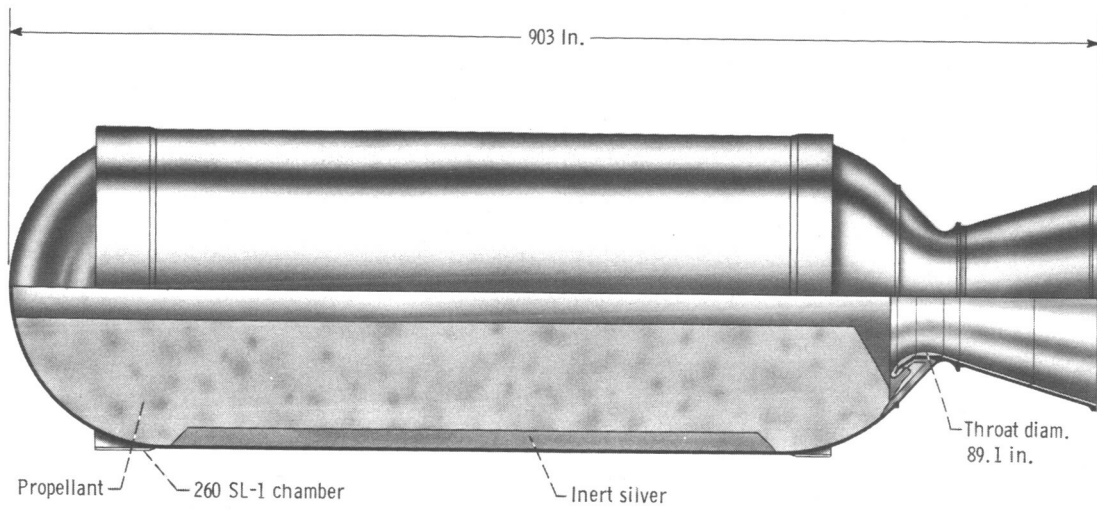
Propellant weight, lb	1,645,000
Inert sliver weight, lb	12,800
Web action time, sec	75.2
Maximum thrust, lb	5,370,000
Average thrust (action time), lb	4,698,000
Maximum pressure, lb/sq in.	600
Average pressure (web action time, lb/sq in.	523
Burn rate (at 600 lb/sq in.), in./sec	.71
Nozzle throat diameter, in.	89.1
Nozzle area ratio	3.78

TABLE II. - MECHANICAL PROPERTIES 260-INCH MOTOR PROPELLANT

	260 SL-1, SL-2*	260 SL-3*
Modulus psi	448	466
Tensile strength S_{NM} , psi	103	85
Strain at maximum stress, m, %	30	21
Strain at break, b, %	35	22

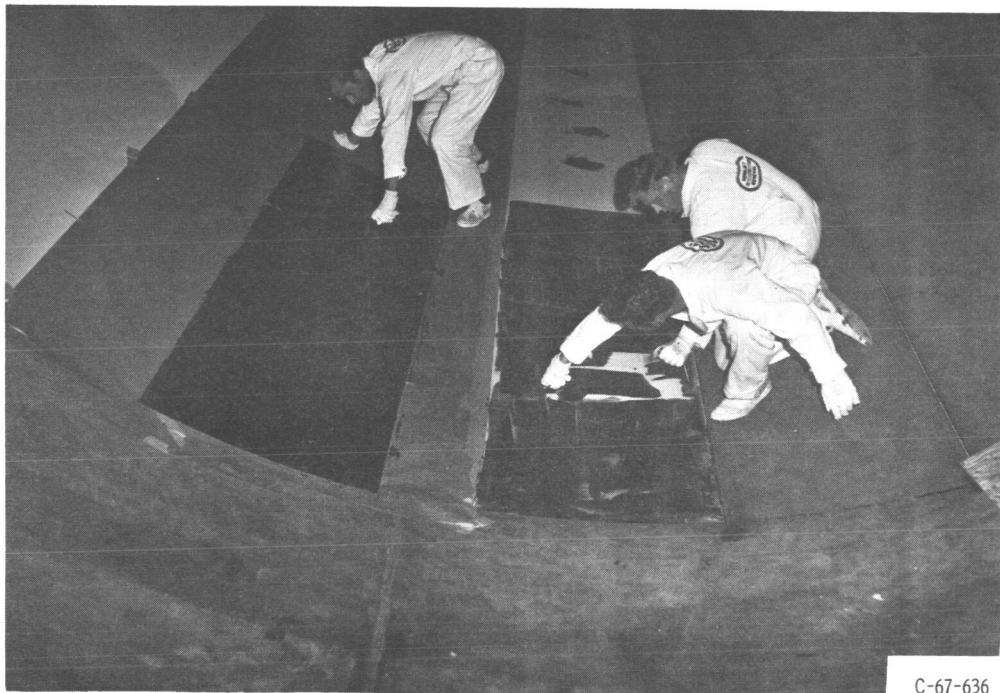
*Representative data for 24-28 day cure, at 77° F.

E-3826



CD-8968

Figure 1. - 260 SL-3 Motor drawing.



C-67-636

Figure 2. - Insulation installation.

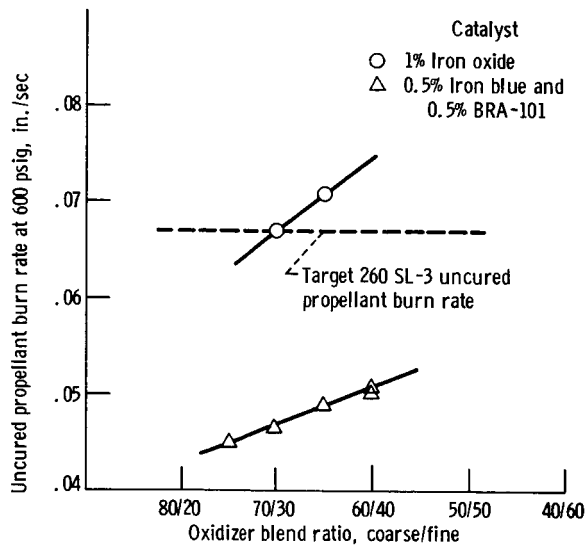


Figure 3. - Effect of catalyst concentration and oxidizer blend ratio on burn rate.

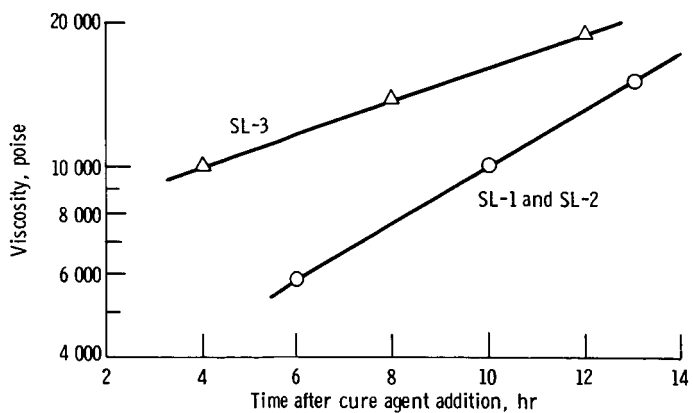


Figure 4. - Viscosity buildup of 260-in. motor propellant.

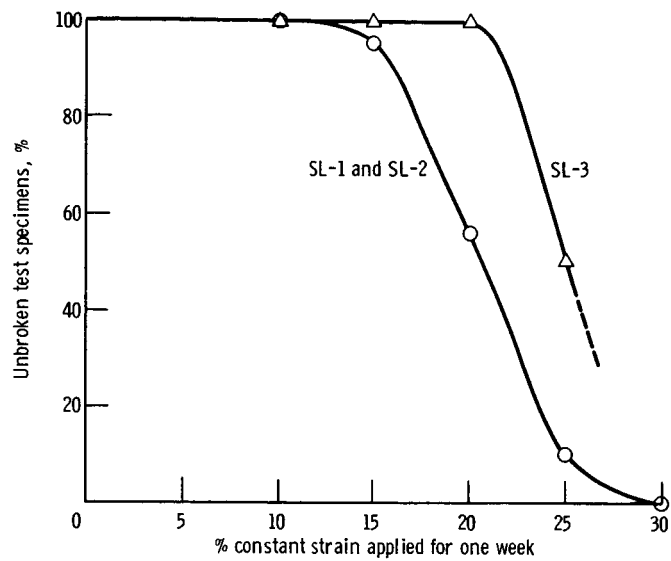
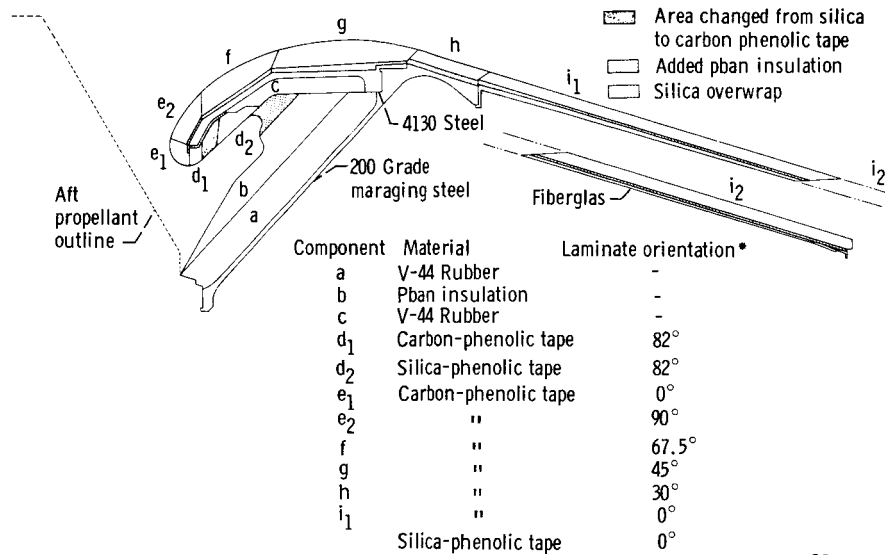


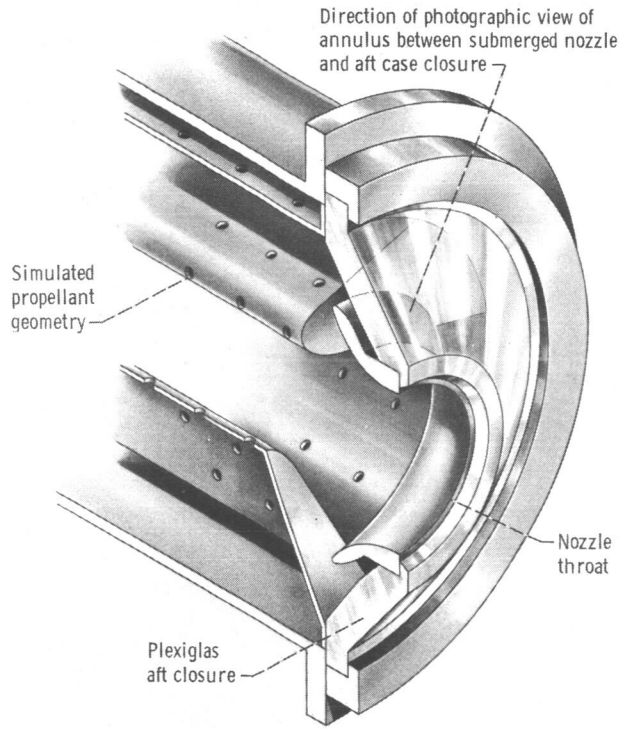
Figure 5. - Constant strain 260-in. motor propellant.



* Laminate orientation from centerline of nozzle measuring from upstream

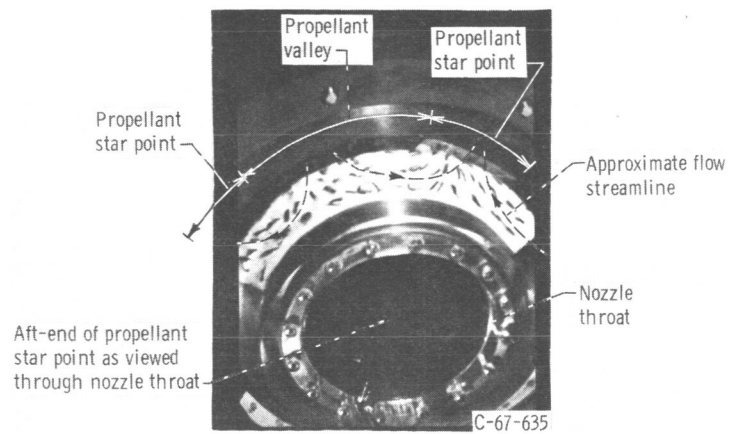
CD-8967

Figure 6. - 260 SL-3 nozzle cross-section.



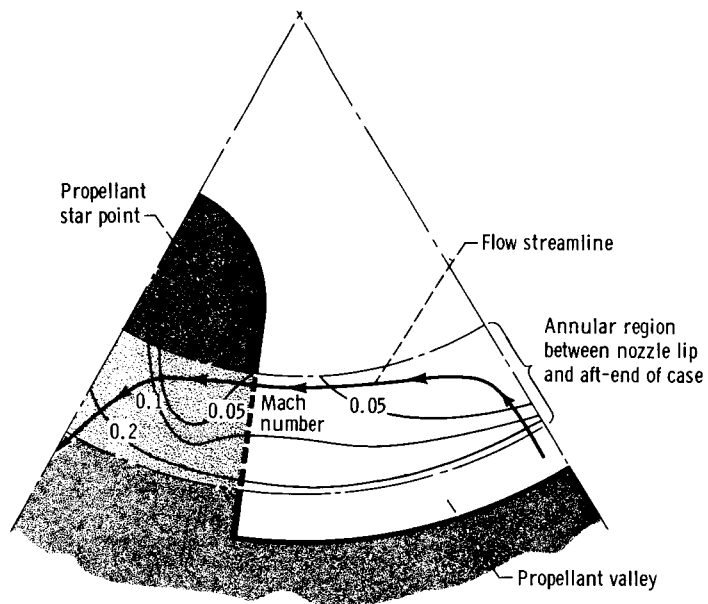
CD-8907

Figure 7. - Schematic diagram of cold-flow test apparatus.



C-67-635

Figure 8. - View of tuft orientation through simulated plexiglas aft-dome of case.



CD-8966

Figure 9. - Mach number profiles behind submerged nozzle entrance section.

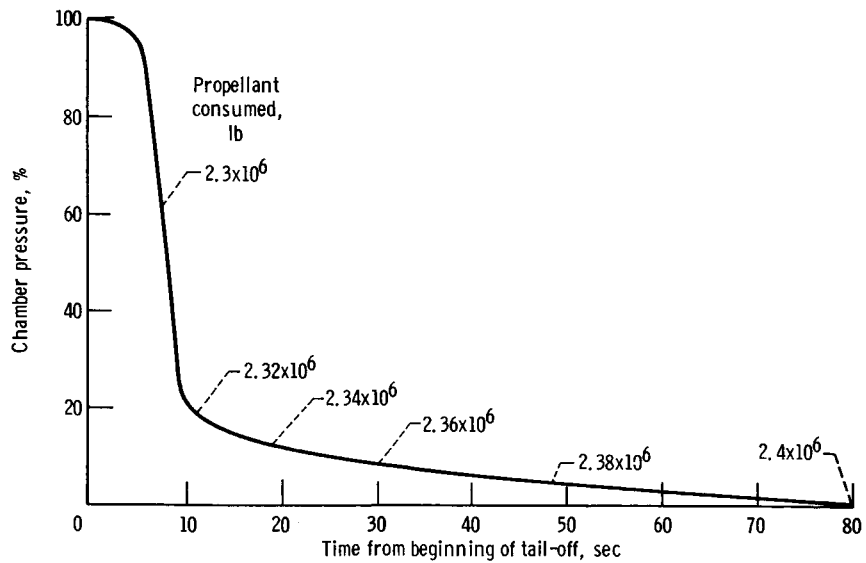


Figure 10. - Motor tail-off used for inert sliver optimization.

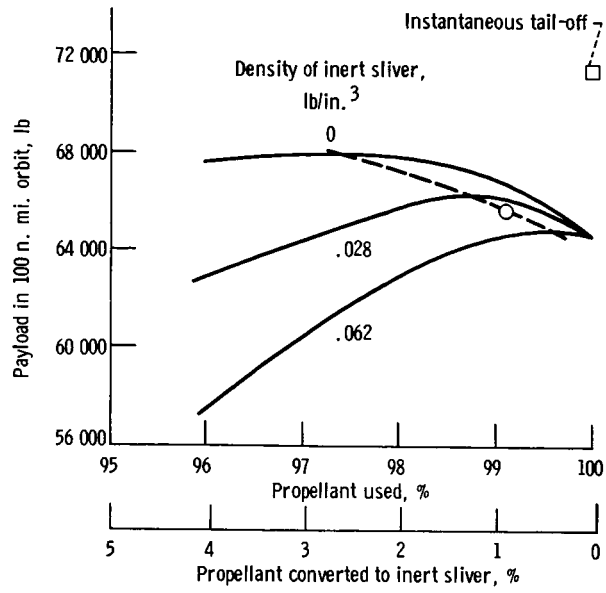


Figure 11. - Effect of propellant inert sliver density and weight on payload.

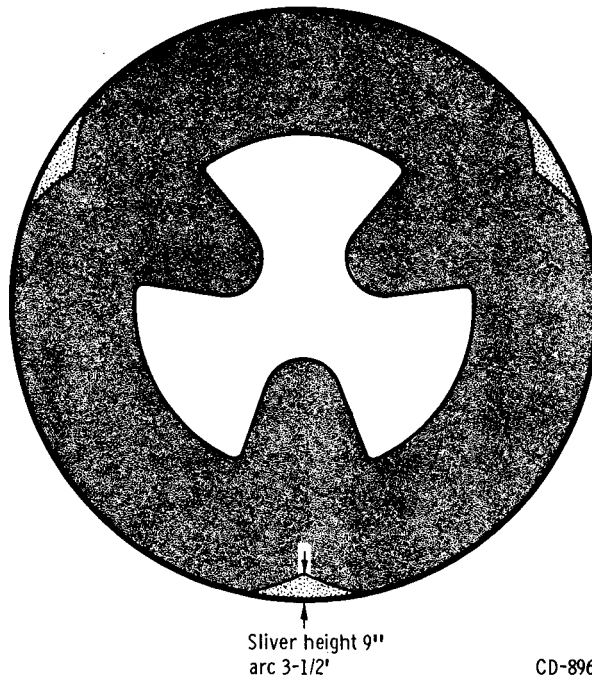


Figure 12. - Cross-section view of slivers.

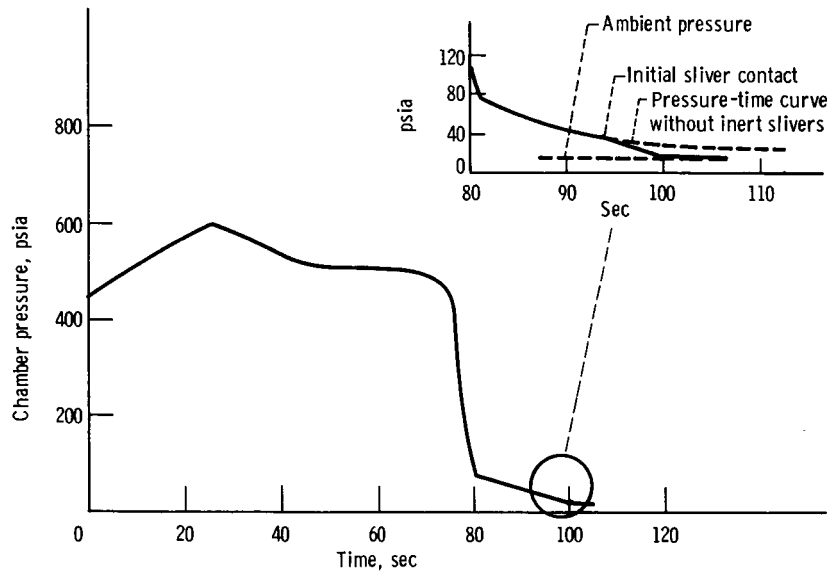


Figure 13. - 260 SL-3 pressure-time curve.